Journal of Mechanical Engineering Research and Developments
ISSN: 1024-1752
CODEN: JERDFO
Vol. 44, No. 2, pp. 47-61
Published Year 2021

Effect Of The Tangential Forces In Contact Interface Of Soft Finger For Grasping And Manipulation

Sadeq H. Bakhy*, Imad A. Abdulsahib, and Enass H. Flaieh

Mechanical Engineering Department, University of Technology - Iraq, Baghdad, Iraq

*Corresponding Author Email: 20093@uotechnology.edu.iq

ABSTRACT: Different models have been investigated for the pressures distribution in the contact interface of a soft finger and an object through the previous studies. Such models have been suggested with no regarding for the influence of the tangential forces that being commonly affected in the contact interface of a soft finger and an object during the grasping and manipulation. Possessing a precise distribution model of pressures through the contact interface is important to develop the friction limit surface (FLS) modeling and design the tactile sensors. In the present research, a newly and highly precise model has been introduced for depicting the pressure distribution asymmetry in the contact interface of hemicylindrical soft fingertip beneath the tangential force and normal force. Such model has been derived depending on the observations in the preceding literature mentioning that the contact interface is moving and skewing to the tangential force direction. Depending on the suggested distribution model of pressure in the current investigation, an enhanced and a highly accurate FLS was introduced. The obtained profile of the FLS via such model was compared with matching outcomes depending upon preceding models. The fresh outcomes displayed that the asymmetry or skewness regard in pressure distribution (owing to the tangential force) leads the profile of the FLS to shrink in comparison with that built with the assumption of the symmetric distribution of pressure. That shrinkage, as a consequence of the asymmetry and skewness of the distribution of pressure, makes the contact interface highly susceptible. Also, the normalized characteristic pitch was not affected by the tangential force. Additionally, such fresh model can also supply more accuracy in different areas, like designing the tactile sensors, haptic perception and enhancing the FLS modeling for the robotic as well as prosthetic hands.

KEYWORDS: Soft finger, Tangential forces, Haptic perception, FLS, Grasping.

INTRODUCTION

Research on dexterous manipulation has been achieved for different purposes: the human skin replacement, the skin-like micro evolution or the soft actuators evolution, the touch sense, the soft manipulation, and so on [1-2]. Within the preceding (2) decades, the anthropomorphic or multifingered robot hands evolution has been tried for reproducing the structure, the shape, the degrees of freedom and, beyond the whole, the human hand functional abilities. The detecting micro-vibrations utilizing the mechanoreceptors at the human hands sensory cells and controlling the power grasping instinctively employing the nervous system are for getting a steady grasp without the damage of objects [3-16]. The tangential torque effect upon the grip forces control, if holding with objects with a precise grip, was introduced by H. Kinoshita at al., 1997 [17]. The tangential force (T) and tangential torque effects were investigated upon the least normal force (N) needed for preventing the slips and upon the normal forces really used via the subjects for holding an object in a static location with the usage of the index finger and thumb tips. It was shown that the normal force increased with the tangential torque. It was also concluded that the minimal normal force required to prevent the slip force reflected T and the frictional circumstance at the object-digit interface. The increment in the utilized normal force with the tangential torque was approximately proportionate with the related increment in the slip force, maintaining a comparatively small safety margin of the normal force for guarding against the unintentional (torsional) slip. Finding the magnitude of the applied moment and force which causes the robotic finger slipping upon the grasped object surface was focused by R. D. Howe et al., 1988 [18]. An enhanced model concerned the torsion-shear interaction. An experimental measurement of soft finger (SF) of an elastomer spherical section and a flat circular specimen (too SF) was introduced for the sliding initiation in terms of loading. Those measurements suggested that a simple linear function of the magnitudes of shear and torsion can predict the slippage in numerous tasks. The outcomes propose (2) practical forms for the limits of friction. A study for the dexterous manipulation modeling using soft contacts (SCs) and stiffness control was presented by Y. Li, and I. Kao, 2001 [19]. The study represents a review of the theories of robotic contact and

contacts models. The model of point contact was determined using Coulomb's friction law, Hertzian contact model, soft contact model, a friction limit surface utilized for modeling the relation between the friction force and the moment at the contacts. The study also introduced the stiffness control approach for modeling and controlling the hands and fingers in dexterous manipulation. It was concluded from the survey that the ellipsoidal limit surface for SF had vacillated the soft fingers analysis in grasping and manipulation and was more realistic analysis in robotics. A technique of constructing the analytical contact models of SFs was presented using the Hertzian model and Winkler basis sharing a number of suppositions concerning the bodies in contact, M. Ciocarlie et al., [20]. Friction constraints were derived using the universal equations of the non-planner contacts of elastic bodies, considering the local geometry and the structure of object in contact. Constraints were expressed as a linear balancing problem; its solution was N and T exerted at every contact in addition to the comparative velocity of the concerned bodies. The used method captured the frictional influences, like the coupling between the T and the frictional torque**.** Those assumptions included a linear relation between the stress and strain, the consistent inner structure of objects, and the minor deformations owing to the contact (comparative to the objects whole size) were modeled using finite element method analysis. The simple contact model of a robotic SF for the power grasping was developed, N. Elango, 2011 [21]. A geometric relation among the contact variables, like deformation, touch angle and contact width, was derived for the cylindrical finger of a soft material. The sliding movements dynamics of a fingerpad upon a smooth class plate was studied, B. Delhaye et al., 2014 [22]. Utilizing a devoted tradition robotic platform, the study appeared the deformation of skin at the area of contact between the finger and the flat surface through the tangential sliding movements onset in (4) various directions (proximal, distal, radial, and ulnar) and with variable N and tangential velocities. A decrease of the area of contact was obtained whilst raising the T and was suggested for explaining such phenomenon via skin's nonlinear stiffening. The shape and amplitude of deformation were extremely reliant on the direction of stimulation. It was also noticed a systematic reduction of the area of contact through the tangential sliding start. Depending upon the Hertzian contact, it was suggested that such variation could be interpreted via the variations in the mechanical characteristics of skin owing to the variation in T. In addition, the stuck area linearly reduced with T, with the slope and the intercept of such relation are vigorously affected via the velocity and N. A review of three approaches of the optimum contact position of the multi-fingered hands was presented, W. Miao, 2015 [23]**;** the geometric analysis-based approach the knowledge rules-based approach, and the optimization-based approach. The grasping force planning was divided into grasping force optimization in the contact force space and the optimization grasping force in the joint torque space. The study concluded that the surface parametrization of the grasped objects was required for the most optimized grasping's which are hard for the irregular objects, also the actual fingers layout needs to be taking into account in the optimization problem, more optimization methods need to be improved. An experimental investigation of the robotic finger stiffness on the maximum resistible force was introduced, F. Fujihira et al., 2015 [24]. A cylindrical fingertip with flat surfaces was utilized in the investigation so as the area of contact stayed the similar if the tangential/shearing force did not exist**.** That was acquired likely for observing the stiffness of fingertip influence further obviously. As well, the contact surface (CS) curvature influence, which wasn't studied in depth, was investigated. The principal results were as following: (1) Harder fingertips make bigger resistible forces, regardless of the CS shape (curved or flat); (2) for the stiffer fingertips, the ultimate resistible force relies greatly upon the shape of CS, whereas for softer fingertips, the shape possesses a slight influence; and (3) for the softer fingertips, the resistible force value varies slightly even if the N raises. A fresh and highly precise model for describing the pressure distribution asymmetry in the contact interface (CI) of the hemispherical SF under the N and T was presented, A. Fakhari et al., 2016 [25]. In relation to the suggested model of pressure distribution in the investigation, an enhanced and highly accurate friction limit surface (FLS) was introduced. The comparison of the obtained profile via the model with the matching preceding models was conducted. The fresh outcomes revealed that the asymmetry and the skewness consideration in the distribution of pressure owing to the Ts cased to shrink the FLS profile in comparison with that resulted with the assumption of the symmetric distribution of pressure, and this shrinkage causes the CI more susceptible. The symmetric and unsymmetric models of the distribution of pressure of the CI of a hemispherical SF beneath the N for constructing the FLS were suggested [23, 26].

No one of the preceding models of the distribution of pressure has regarded the influence of the tangential forces (TFs) that being frequently applied in the CI of a hemicylindrical soft fingertip (HSFT) and an object through the grasping and manipulation (Figure. 1), [27]. Thus, in the present investigation, a fresh expression was proposed for the distribution of pressure in the CI of a HSFT beneath both the N and T depending on the findings of the preceding experimental investigations [28, 29]. However, such aspect has not been confirmed by any previous research. Such model being the expansion as well as the enhancement of preceding models of the distribution of pressure [30, 26] and can be employed in various areas, like designing the tactile sensors, haptic perception, and the construction of a highly precise FLS. Therefore, an enhanced FLS is introduced depending on the suggested model of the distribution of pressure in the current investigation.

`

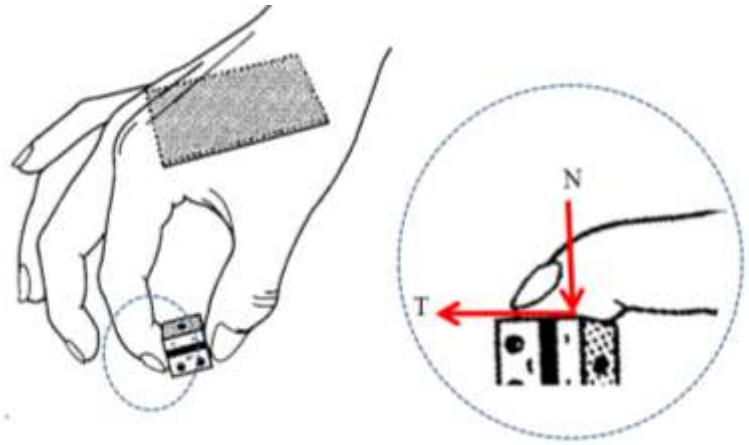

Figure 1. An anthropomorphic SF under N and T [27]

MODELS OF THE SOFT CONTACT (SC)

The agreeable manipulation and grasping analysis is based highly upon the modeling of a good contact mechanics. The model of soft contact must be employed when the deformation is not negligible. Human fingers softness can expand the dexterous manipulation and stable grasp. Researchers have been proposed many soft contact models. The models of contact are classified into the linear elastic models and the nonlinear elastic models. Model of Hertzian contact is the first linear elastic one. In 1882, the model of Hertz was investigated experimentally for a slight deformation in contact between a rigid plate and a linear elastic material hemisphere [31]. Based on the linear elastic model, the Hertz model states that the radius of circular contact area is proportionate to the N raised to power (1/3). The model of Hertzian contact isn't convenient for the big deformation of the nonlinear elastic materials experimentally revealed via Tatara [32]; that is, when the ratio of the contact area radius to the hemispherical soft fingertip radius is greater than 0.3. After that, Timoshenko and Goodier [33] presented the contact between (2) parallel cylinders and they obtained analytically that the half width contact value (a) for a linear elastic cylinder is proportionate to the N raised to power (1/2), (i.e. $a \propto N^{\frac{1}{2}}$).

The time-dependent or viscoelastic models and the time-independent models are classified for nonlinear contact models. A time-independent contact model considers the power-law model. Based on the theory of mechanics with the investigational confirmation, such model was developed [34], where it subsumes that the contact model of Timoshenko and Goodier as the half width contact value (a) for a linear elastic cylinder is a coefficient (c) multiplied by N raised to power (γ), (i.e. $a = c\,N^{\gamma}$), where γ is equal to (n/(n + 1)), n is the strain-hardening constant, and c being a constant relying upon material characteristic size as well as the soft fingertip (SFT) curvature. Because n possesses values in the range ($0 \leq n \leq 1$), therefore γ possesses values in the range of ($0 \leq \gamma \leq 1/2$). The constant (n) equals one (i.e., γ is 1/2) for the linear elastic substances, resulting in the model of the contact of Timoshenko and Goodier. Depending upon theory of power-law, I. Kao and F. Yang [35] investigated the contact nonlinear stiffness for the hemispherical soft fingertips. Other significant models of the time-independent SC comprise the model of radial distribution suggested via S. Arimoto et al. [36], the suggested model of linear spring/damper via Kim [37] as well as the offered model of parallel-distribution via Inoue and Hirai [38, 39]. In the models of the time-dependent or viscoelastic contact, phenomena of the creep and the relaxation are noted within the soft substances. The first viscoelastic contact models based on springs and dampers in series and parallel are proposed; the model of Kelvin-Voigt [40] and the model of Maxwell [41]. Another viscoelastic model founded upon the split-up of the temporal and the elastic outputs was modeled via Fung [42], and Kao and Tiezzi [43, 44] simplified such model for presenting a visco-elastic model for the CI of robot.

PRESSURE DISTRIBUTION BENEATH NORMAL CONTACT FORCE

The distribution of pressure upon a rectangular contact area (RCA) between a rigid plate and a HSFT with a linear elastic material based on the Timoshenko and Goodier contact model [33] is a profile as:

$$p = \frac{N}{\pi\, a\, l}\ \sqrt{1 - (\frac{y}{a})^2} \qquad (1)$$

Where:

N: Normal contact force

a: The half width contact value of a RCA for a HSFT

y: Distance from contact center with $0 \leq y \leq a$

l: Half depth of rectangular contact

The profile of pressure distribution becomes more uniform when the soft hemicylinder material properties in the contact zone (region) change into hyper-elastic ones. Therefore, the broad function of pressur distribution (PD) for a RCA was introduced [45], which includes the Timoshenko and Goodier's formula in Eq. 1 as:

$$p = C_k \frac{N}{2\pi\, a\, l} \left(1 - (\frac{y}{a})^k\right)^{\frac{1}{k}} \quad (2)$$

Where, k determines the profile shape of pressure, and ($C_{k)}$ is constant for the PD profile above the contact area to be suitably in an equilibrium state; that means the pressure integration (p) over the rectangular area of contact equals the contact normal force (N). C_k can be got as:

$$C_k = \pi \frac{k\, \Gamma\left(\frac{2}{k}\right)}{\left[\Gamma\left(\frac{1}{k}\right)\right]^2} \;,\quad k = 1, 2, 3, \cdots \quad (3)$$

Where, Γ( ) is the function of Gamma [46]. In the Eq. 2, if k is equal to two, the model of the pressure distribution of Timoshenko and Goodier, in Eq. 1 is determined. Via raising the parameter k, the profile of the distribution of pressure gets highly homogenous [45,47,48].

THE CONTACT DISTRIBUTION OF PRESSURE BENEATH N AND T

The Deformation of The Area of Contact

If a T is exerted at a soft CI, an incomplete slip can happen via raising the T initially lengthwise the area of contact boundary and prevailing towards the inside of the area of contact, and after that, the gross slip shall take place if the CI can no lengthier withstand the comparative movement at surface. During the partial slip, the CA being split into (2) zones : (1) slip zone, where an incomplete slip takes place and (ii) stick zone, where the object doesn't travel comparative to fingertip. Cattaneo in (1938) [49] and Mindlin in (1949) [50] solved the incomplete slip problem in the contact zone between a pair of elastic spheres beneath N and T. The Hertzian distribution of pressure in CI with fixed magnitudes was assumed. Moreover, they assumed by conservation the contact N constant and raising the contact T from (0) homogeneously, the microslip starts instantly at the edge of CA, also it propagates towards the center of CA, as displayed via

$$\acute{a} = a \left(1 - \frac{T}{\mu\, N}\right)^{\frac{1}{3}} \quad (4)$$

Where:

$\acute{a}$: The effective radius of the area of stick

If (T) approximates (μN), the area of stick will shrink to a point in the center of CA, and then the gross slip initiates [49]. Moreover, the elastic object deformation (δ) was investigated beneath the (T), utilizing the theory of Hertz prior to the occurrence of gross slip. This can be introduced by the experiment [51] as:

$$\delta = \frac{3\mu N}{16\, a} \left(\frac{2-v}{G}\right) \left[1 - (1 - \frac{T}{\mu N})^{\frac{2}{3}}\right] \quad (5)$$

Where:

μ: Coefficient of friction between an elastic object and a rigid plate.

v: Poisson's ratio.

G = E / (2 + 2 v) being the shear modulus.

E: Modulus of elasticity of the elastic object (Young's modulus)

Kurita et al. introduced the area of contact deformation beneath the N and T for the hemispherical soft objects [28, 29] as well as the human fingertips [52, 53]. Their investigational study supposed the distortion of soft object, and the zone of stick movement in the direction of (T), as depicted in Figure. 2.

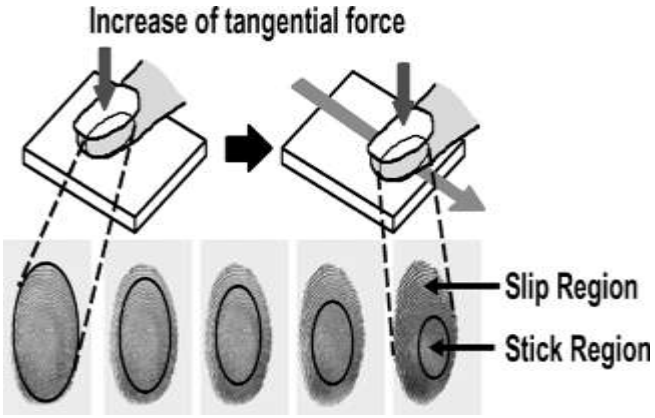

Figure 2. Deformation of the area of contact founded upon the Kurita's experimental study [52, 53]

The Skewness in The Distribution of Pressure

In relation to the investigational works and observations of Kurita, one can deduce that if a T is raised upon a SF beneath a N, the microslip starts from the edge of CA, where pressure is the least, then it propagates towards a point having an ultimate pressure at stick zone center (Figure. 2). Since the zone of stick moves to the tangential forces (TF) direction, practically, the distribution of pressure in the area of contact skewed consequently, as displayed in the Figure. 3. A schematic of a HSFT beneath the normal contact force and tangential contact force prior to the occurrence of gross slip is evinced in Figure. 4, where f_t is the tangential frictional force, and $f_t = T$. The distribution of pressure skewness being needful for the moment resulted via f_t and T for balancing the moment resulted via the contact (N) and the distribution of pressure, $p(y)$.

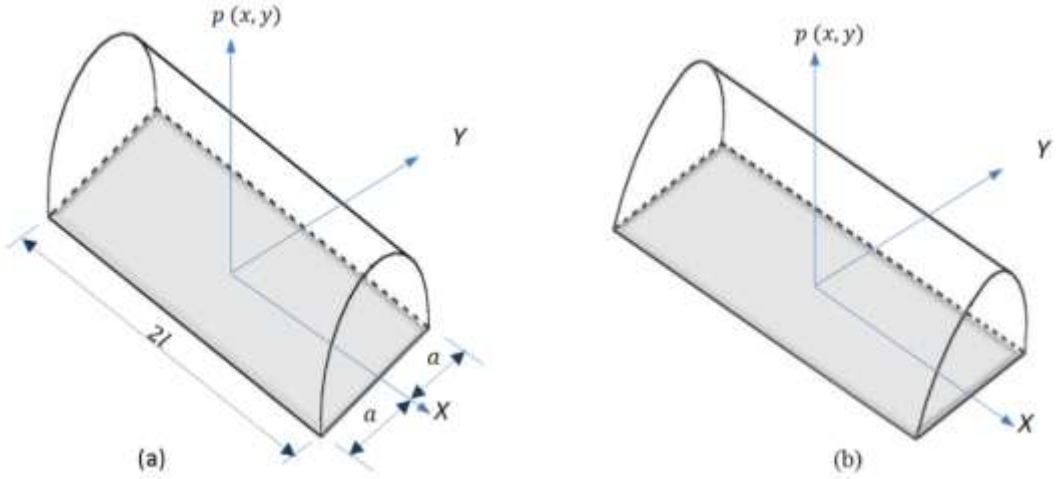

Figure 3. Profile of the distribution of pressure of a HSFT beneath the N: **(a)** Before exerting T, and **(b)** After exerting T

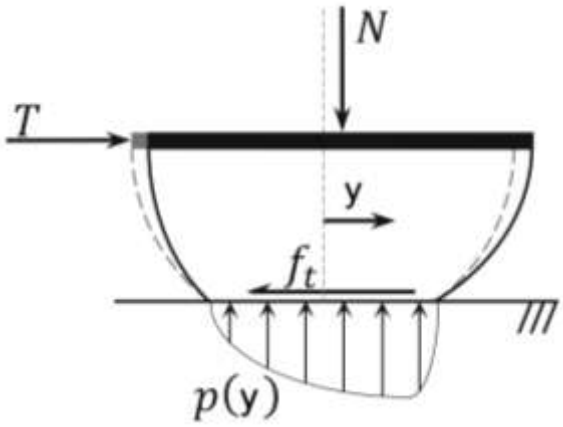

Figure 4. A schematic of a HSFT cross section beneath the N and T

Here, a model for representing the skewness within PD being evolved. A HSFT under N and T and its area of contact are evinced in Figure. 5 in which the Cartesian coordinates (X', Y) being devoted to a point having an ultimate pressure (O'), and it is positioned at point (X', Y) respecting to centroidal Cartesian coordinates (X, Y). In this study, the Ts cause a deformation in the y-axix only; that means $\Delta x = 0$. Every point upon the area of contact boundary, for example, (C) in the Figure. 5b can be clarified with regard to the relationship between ρ and the half width contact of RCA for a HSFT, a, based on the geometry of OOC is represented as ρ can be calculated s

$$\boldsymbol{\rho = a - \Delta y} \tag{6}$$

By using the broad form in the Eq. 2, the SPD of pressure skewness being introduced as:

$$\boldsymbol{p = A \left(1 - (\frac{y}{\rho})^k\right)^{\frac{1}{k}}} \tag{7}$$

Where, $0 \leq y \leq \rho$, and (A) is a constant modifing for the skewness PD profile of for satisfying the state of equilibrium. Therefore, (A) is written in form:

$$A = \frac{N}{\int_{-l}^{+l}\int_{-a}^{+a}\left[1 - (\frac{y}{\rho})^k\right]^{\frac{1}{k}} dy\, dx} \tag{8}$$

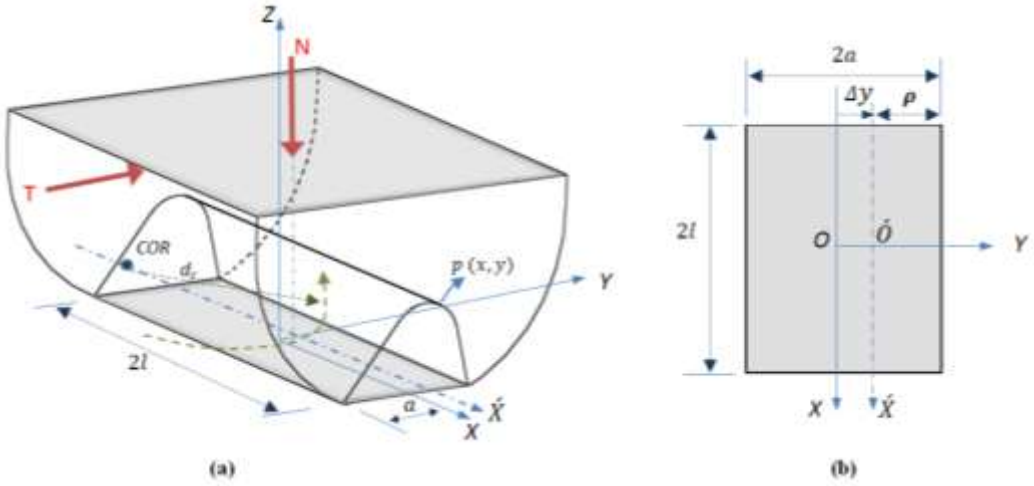

Figure 5. (a) SF beneath the N and T, (**b)** Cartesian coordinates *(X, Y)* and *(X', Y)* representation in the CA

Via varying (k) and (Δy) in the Eq. 8, the outcomes demonstrate that (A) is a feeble function of (Δy). Thus, (A) can be computed via the negligence of (Δy) in the Eq. 6 with no generality loss. Therefore, an equation for representing the distribution of pressure skewness is suggested as:

$$p = C_k \frac{N}{2\pi\, a\, l}\left[1 \quad - \quad (\frac{y}{\rho})^k\right]^{\frac{1}{k}} \tag{9}$$

Where, C_k is defined in Eq. 3. The normalized distribution of pressure, $p/(N/(2\pi al))$, with regard to the normalized half width contact of RCA for HFTs (y/a) when ($k = 2$) and ($\Delta y\ /a = 0.5$), is drawn in the Figure. 6. The suggested model of the distribution of pressure can be used in various applications, like the haptic insight, the designing of tactile sensors as well as the enhancing of the modeling of FLS modeling for robotic and prosthetic hands.

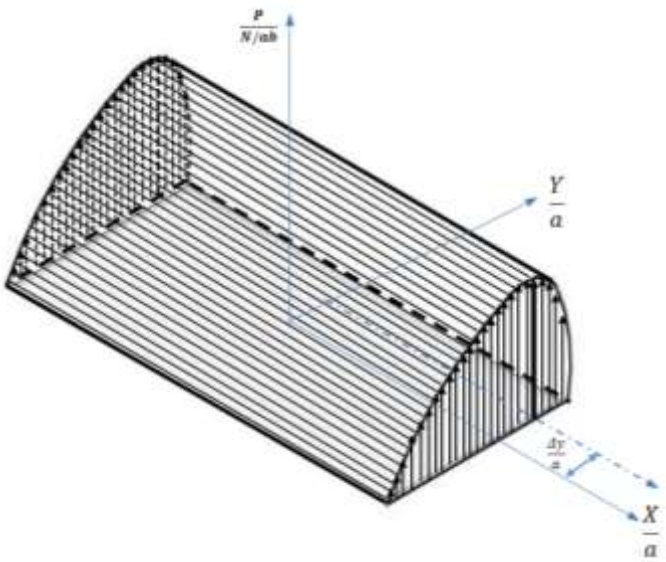

Figure 6. The normalized distribution of pressure with regard to the normalized radius

FRICTION LIMIT SURFACE USING THE SKEWED DISTRIBUTION OF PRESSURE

In place of friction cone in a point contact, friction limit surface [19, 45, 54, 55] for a soft contact being known. Because the frictional moment is applied at soft CI lengthwise with N in addition to T, FLS being utilized for finding if the gross slip initiates between object and SF. Thus, if the (f_t) and frictional moment (m_n) in the area of contact being in the FLS boundary, no comparative movement within the contact exists. By f_t as well as m_n rising toward the FLS boundary, the slippage in contact begins. Really, FLS is characterized as mapping between sliding motions and contact forces/moment numerically built the FLS for a HSFT under a N utilizing the distribution of pressure that is introduced in Eq. 2 [26] without regarding skewness within PD if T being exerted. They approached the FLS via an ellipse having a minor axis and a major axis as an ultimate tangential frictional force ($f_{t_{max}} = \mu N$) and an ultimate frictional moment normal to CA, $(m_n)_{max}$, correspondingly in this equation:

$$\frac{{f_t}^2}{(\mu N)^2} + \frac{{m_n}^2}{(m_n)^2_{max}} = 1 \tag{10}$$

Where, (μ) is the coefficient of the friction of contact. Being explained in prior section, the distribution of pressure skews if a T is exerted. In the Figure. 7, the RCA of a HSFT in gross slip condition with its instantaneous center of rotation is seen. With no generality loss, the center of rotation is regarded alongside *X*-axis. Via varying the location of the center of rotation; that means the distance (d_c) from origin to (+ ∞) alongside *X*-axis, various conditions of slippage are acquired for constructing the FLS. The f_t over the rectangular area of contact (Ω) can be calculated via integrating the shear stress ($\boldsymbol{\tau}$) over the infinitesimal areas ($d\Omega$) as:

$$\mathbf{f}_t = \int_\Omega \boldsymbol{\tau}\, d\Omega \tag{11}$$

Likewise, (m_n) can be got as:

$$\mathbf{m}_n = \int_\Omega (\boldsymbol{r} \times \boldsymbol{\tau}) \, d\Omega \tag{12}$$

Where $\boldsymbol{\tau} = -\mu \, p \, (y) \, \bar{\mathbf{v}}$ being the shear stress upon the rectangular CI of SF as well-defined in relation to the law of Coulomb and is in an opposing to the normalized unit vector ($\bar{\mathbf{v}} = \frac{\mathbf{v}}{|\mathbf{v}|}$) direction respecting to center of rotation (Figure. 7b), where **(v)** is the vector velocity of an infinitesimal element of CA, *d*Ω, which it would possess if gross slip begins, and *p(y)* is the SFD. Equation 11 and Eq. 12 can be expressed using Eqs. 6 and 9 as:

$$\mathbf{f}_t = -\frac{\mu C_k N}{2\pi \, a \, l} \int_\Omega \left(1 - \left(\frac{y}{\rho}\right)^k\right)^{\frac{1}{k}} \bar{\mathbf{v}} \, d\Omega \tag{13}$$

$$\mathbf{m}_n = -\frac{\mu C_k N}{2\pi \, a \, l} \int_\Omega \left(1 - \left(\frac{y}{\rho}\right)^k\right)^{\frac{1}{k}} \boldsymbol{r} \times \bar{\mathbf{v}} \, d\Omega \tag{14}$$

Where, the normalized velocity vector ($\bar{\mathbf{v}}$) is computed as:

$$\bar{\mathbf{v}} = \frac{1}{\sqrt{x^2 + (d_c - y)^2}} \begin{bmatrix} -y \\ x - d_c \end{bmatrix} \tag{15}$$

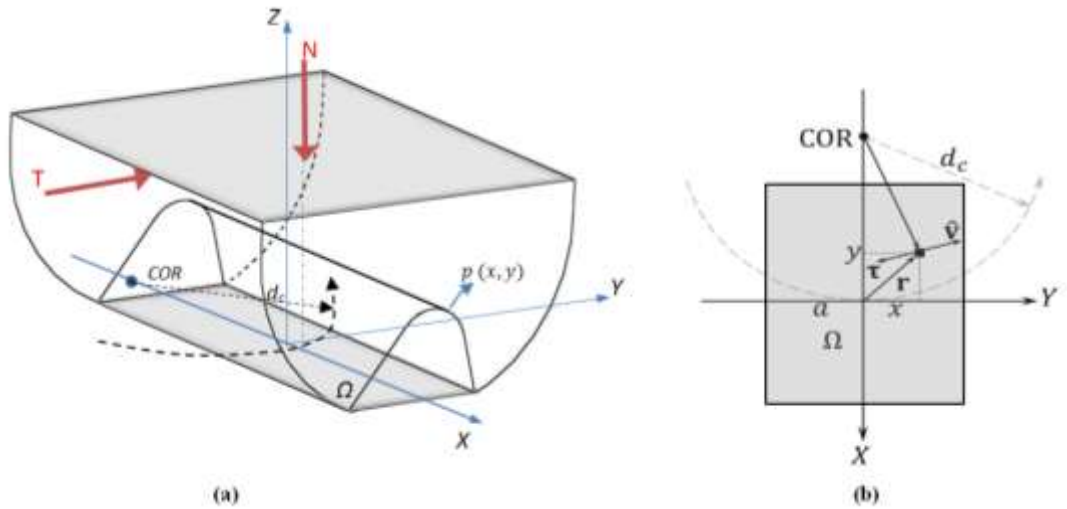

Figure 7. (a) The contact area of the SF in the condition of gross slip and its instant center of rotation (COR) of a HSFT, and (**b)** Diagram of contact area upon the plane of (*XY*)

The parameters Δ_x on Y-axis symbolize the point with the maximum pressure (P_{max}) depending upon the property of material of soft fingertip in addition to the exerted T direction and magnitude. For solving the (2) integrals of Eq. (13) and Eq. (14) to construct the FLS, a relationship between the point location with P_{max} and d_c is wanted. In Figure. 8, the point locus with P_{max} and the f_t, if the center of rotation moves from the origin to (+ ∞) alongside the *X* –axis, being displayed upon the CI of the HSFT depicted in Figure. 7a. If the center of rotation being within the origin ($d_c = 0$), then $f_t = 0$ and there's no skewness in the distribution of pressure. If the center of rotation goes to + ∞ ($d_c \rightarrow + \infty$) alongside the *X* –axis, $f_t = -\mu N \, \hat{\imath}$ and the point with P_{max} shifts toward $\Delta_x = \Delta$, as shown in Figure. 8. The unit vector ($\hat{\imath}$) being alongside the positive *X*-axis, also the parameter (Δ) is the ultimate PD profile skewness in the SFT contact. Because the PD skews toward the positive *Y*-axis, the τ for the elements upon right-half plane being greater than left-half plane; that means $|\tau_1| < |\tau_2|$. Therefore, when d_c moves from zero to (+ ∞) alongside the *X* -axis, $f_t = f_i^x \, \hat{\imath} + f_j^y \, \hat{\jmath}$, and it varies from zero to ($-\mu N \hat{\imath}$), where $f_i^x \leq 0$ and $f_j^y \leq 0$ (Figure. 8). Consequently, the point with P_{max} that shifts from origin to ($\Delta_x = \Delta$) upon a path within 1st quadrant of the lane of (*XY*), as revealed in the Figure. 8. Such path can be expressed as an elliptical one with

$$\Delta x = \frac{h}{\Delta/2}\sqrt{\left(\frac{\Delta}{2}\right)^2 - \left(\Delta y - \frac{\Delta}{2}\right)^2}\ . \quad (16)$$

Where, h and Δ/2 are the both minor axis and major axis length, correspondingly. A relationship between the location of point having P_{max} and d_c is proposed in such a way that when $d_c = 0$, $\Delta y = 0$ and when $d_c \rightarrow +\infty$, $\Delta y = \Delta$, as follows:

$$\Delta y = \Delta \tanh(\alpha\, dc) \quad (17)$$

Where, $\tanh$ is the hyperbolic tangent function, also α being constant that's chosen in order that the convergence rate of (Δy) to (Δ) being alike that the convergence of $|\boldsymbol{f}_t|$ to μN if the center of rotation shifts from origin to $(+\infty)$. A closed-form resolution for the Eq. (13) and Eq. (14) integrals doesn't occur, but it can be numerically analyzed for constructing the FLS via normalizing them as:

$$\frac{\mathbf{f}_t}{\mu N} = -\frac{C_k}{2\pi\, a\, l}\int_{-1}^{+1}\int_{-1}^{+1}\left(1-\left(\frac{\bar{y}}{\bar{\rho}}\right)^k\right)^{\frac{1}{k}}\bar{\mathbf{v}}\ d_x\ d_y \quad (18)$$

$$\frac{\mathbf{m}_n}{\mu N a} = -\frac{C_k}{2\pi\, l}\int_{-1}^{+1}\int_{-1}^{+1}\left(1-\left(\frac{\bar{y}}{\bar{\rho}}\right)^k\right)^{\frac{1}{k}}\begin{pmatrix}\bar{x}\\ \bar{y}\end{pmatrix}\times\ \bar{\mathbf{v}}\ d_x\ d_y \quad (19)$$

where $\tilde{x} = \frac{x}{l}$, $\tilde{d}_c = \frac{d_c}{a}$, $\tilde{y} = \frac{y}{a}$, $\tilde{\Delta}x = \frac{\Delta x}{l}$, $and\ \tilde{\Delta}y = \frac{\Delta y}{a}$

$$\tilde{\rho} = 1 - \tilde{\Delta}y \quad (20)$$

$$\bar{\bar{\mathbf{v}}} = \frac{1}{\sqrt{\tilde{x}^2+(\tilde{d}_c-\tilde{y})^2}}\begin{bmatrix}-\tilde{y}\\ \tilde{x}-\tilde{d}_c\end{bmatrix} \quad (21)$$

The numerical integration results via shifting the location of the center of rotation (d_c) from origin to $(+\infty)$ alongside the *X*-axis for the skewed PD and the non-skewed PD ($\Delta x = \Delta y = 0$) [25] in addition to an elliptical approximation, Eq. (10), being depicted in Figures (9 to 11) with regard to the normalized force ($\frac{|\mathrm{f}_t|}{\mu N}$) and the normalized moment ($\frac{|\mathrm{m}_n|}{\mu N a}$).

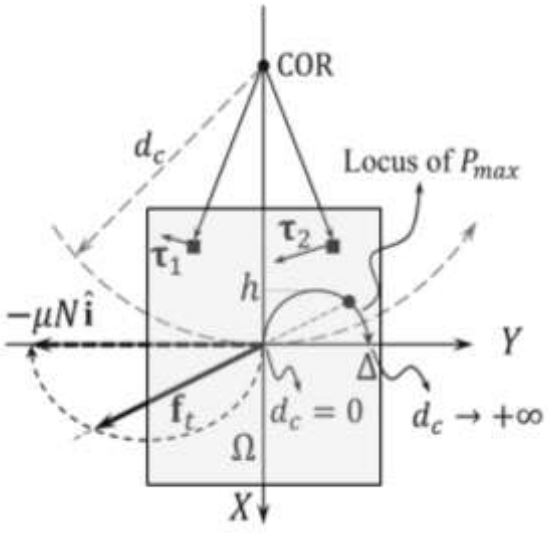

Figure 8. The point Locus with *Pmax* and $\boldsymbol{f}t$ if the center of rotation moves from origin to (∞) alongside the *X*-axis upon the CI of the HSFT depicted in the Figure. 7a

RESULTS AND DISCUSSION

The outcomes evinced in Figures (9 to 11) display that the FLS profile considering the skewness in the PD, to the T, being positioned within the profile of FLS without considering the skewness in the PD. Also, the outcomes cause a sense since the skewness of the PD owing to that the T shall create the CI more susceptible; thus, the FLS profiles being anticipated to move inside. From Figures (9 to 11), if the PD gets more homogenous with bigger *k* values, Kao [26], its skewness owing to the TF gets less important and the outcomes in the less inside movement of the FLS. The discrepancy between the profiles of FLS with and without regarding the skewness of the PD for least possible (k), i.e., k is equal to (2) causing a model of the Hertzian PD, is less than (4.01%) for the normalized T and (1.05%) for the normalized (m_n) (Figure. 9). From the other side, when dc is zero, the normalized moment approximates its ultimate values (0.7114 when k is 2, 0.7442 when k is 4, and 0.7649 when k is 50). The typical pitch of a soft contact ($\tilde{\lambda}$), too significant in the SF modeling and kinematic relations [26], is well-defined as the ratio between the mn_{max} and $f_{t_{max}}$, as elucidated in the SF limit surface, thus, the normalized typical pitches of SFs founded upon the normalized limit surface is:

$$\tilde{\lambda} = \frac{m_{n_{max}}/a\mu N}{|f_{t_{max}}|/\mu N} = \begin{matrix} 0.7114 & \text{if k is 2} \\ 0.7442 & \text{if k is 4} \\ 0.7649 & \text{if is 50} \end{matrix} \quad (22)$$

No effect of TF being observed on the characteristic pitch of HFTs.

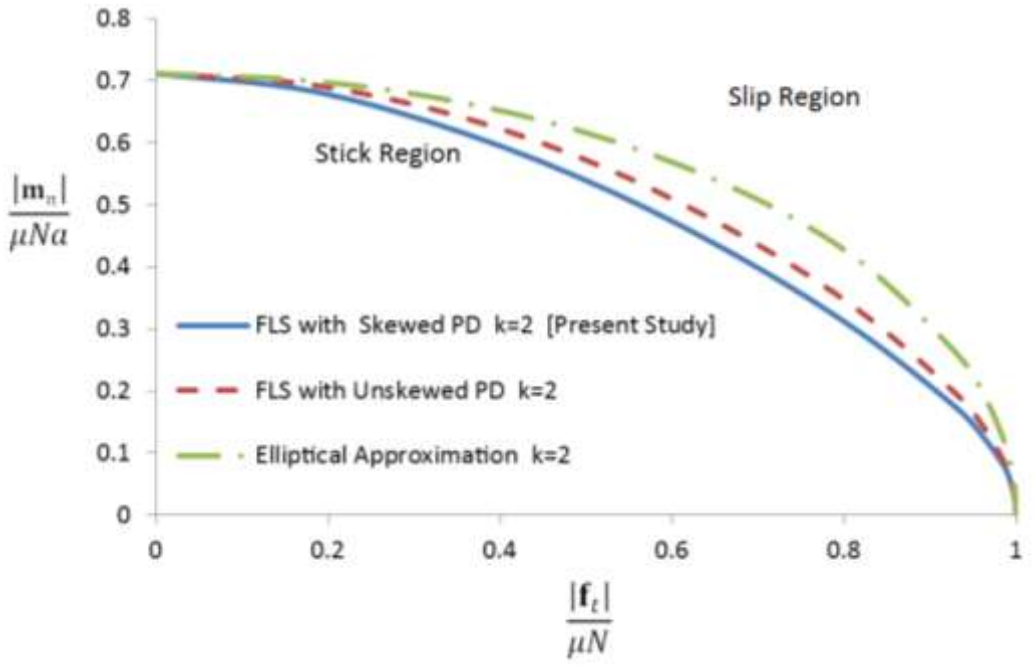

Figure 9. Friction limit surface (FLS) with skewness [present study] and without regarding the skewness [45] in the distribution of pressure (PD) when (*k*) is (2) and (4) with (Δ/a) is (0.9), (α) is (1.1), and a circular path for P_{max} locus (*h* is $\Delta/2a$)

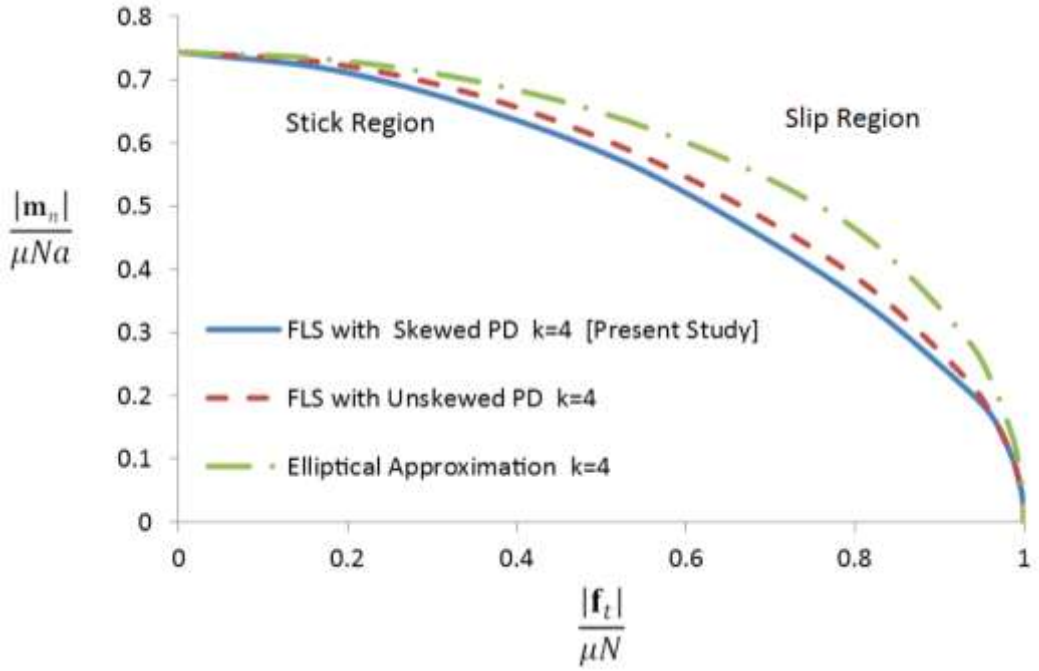

Figure 10. Friction limit surface (FLS) with skewness [present study] and without regarding the skewness [45] in the PD when *k* is 4 with (*Δ/a*) is (0.9), (*α*) is (1.1), and a circular path for P_{max} locus (*h* is *Δ/2a*)

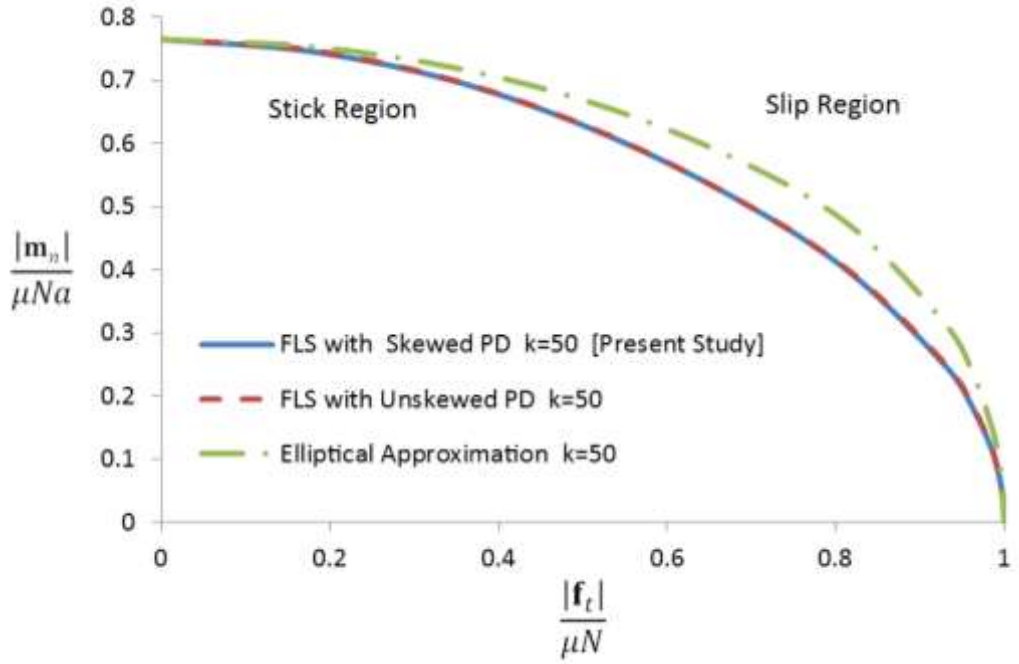

Figure 11. FLS with skewness [present study] and without regarding the skewness [45] in distribution of pressure (PD) when (*k*) is (2) and **(**50) with (*Δ/a*) is (0.9), (*α*) is (1.1), and a circular path for P_{max} locus (*h* is *Δ/2a*)

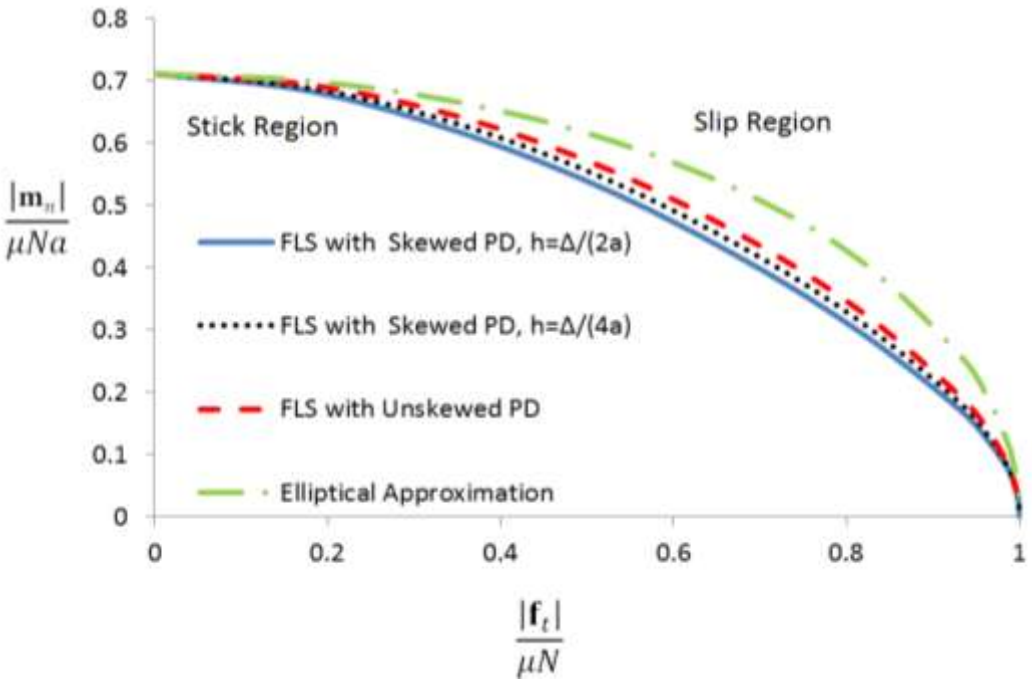

Figure 12. Friction limit surface for two positions of P_{max} with Δ/a = 0.9, α = 1.1, and k = 2

Moreover, various P_{max} loci, displayed in the Figure. 8, being used for investigating the influence of this supposed locus upon the limit surface. By the explanation in the Figure. 12, the P_{max} locus size possesses unimportant influence upon the limit surface outcomes. This proposes that the outcomes presented now aren't sensitive to the variations in the utilized parameters in modeling, and they can be generalized for the soft CI modeling in the manipulation and grasping. In concise, FLS is the feeble function of PD skewness, and the difference between the FLS profiles with and without regarding the PD skewness being unimportant. The regard of T and the resulted skewed PD within CI possess unimportant effect upon the total FLS in comparison with the FLS with the unskewed CI in the present literature, though causing too somewhat slippage susceptibility, as anticipated. Accordingly, a FLS built via the assumption of the symmetric PD in the CI, which is straight and simple to build, being sufficient for the SCs modeling in the robotic manipulation and grasping. Therefore, a symmetric distribution of pressure in the CI is adequate for the FLS modeling of a soft contact. Such model can be utilized in different areas, like designing the tactile sensors, the haptic perception, and enhancing the FLS modeling for the prosthetic and robotic hands [56-74].

CONCLUSION

Via implementing a T and N at a HSFT, the area of contact distorts and splits into (2) zones: slip zone and stick zone. In relation to the notes in the preceding literature, if the T rises, the stick zone in the RAC contracts and moves toward the exerted force direction. Consequently, the PD in the CI skews also. Thus, a general model for describing the PD asymmetry through the soft contacting interface with T beneath N was suggested. In relation to the suggested model of the PD in the present investigation, an enhanced and more precise FLS was introduced. A significant inquiry to reply, beneath such circumstance, is whether this skewness in CI will possess a large participation to the FLS. The outcomes of such investigation manifested that the FLS is a little function of SPD in CI. The regard of T and resulted skewed PD in the CI possess unimportant effect upon the general FLS in comparison with the FLS with unskewed CI in the present literature, though causing too somewhat slippage susceptibility, as anticipated. In addition, the normalized typical pitch wasn't influenced via the T. Accordingly, a FLS built via the assumption of the symmetric PD in the CI, which is straight and simple to build, being suitable for the SCs modeling in the robotic manipulation and grasping.

REFERENCES

[1] T. Okada, "Object handling system for manual industry," IEEE Tran. on Syst. Man Cybern Vol. 9, No. 2, pp. 79–89, 1979.

[2] J. K. Salisbury, and J. Craig, "Articulated hands: force control and kinematic issues," Int. J. Robot Res. Vol. 1,

pp.4–17, 1982.
[3] N. Munro, F.L. Lewis, and C.T. Abdallah, "Robot manipulator control theory and practice," Marcel Dekker, Inc. Second Edition. 2004.
[4] R. Johansson, and G. Westling, "Roles of glabrous skin receptors and sensorimotor memory in automatic control of precision grip when lifting rougher or more slippery objects," Exp. Brain Res. Vol. 56, No. 3, pp. 550–564, 1984.
[5] R. Johansson, and G. Westling, "Signals in tactile afferentsfrom the fingers eliciting adaptive motor responses during precision grip," Exp. Brain Res. Vol. 66, No. 1, pp.141–154, 1987. Doi:10.1007/BF00236210.
[6] M. A. Jabbar, Sadeq H. Bakhy, and E. H. Flaieh, "An experimental study for grasping and pinching controls for an underactuated robotic finger using a PID controller" , IOP Conference Series: Materials Science and Engineering 433, 2018.
[7] M. A. Jabbar, Sadeq H. Bakhy, and E. H. Flaieh, "A new multi-objective algorithm for underactuated robotic finger during grasping and pinching assignment," IOP Conference Series: Materials Science and Engineering 671, 2020.
[8] S. K. Mahmood, Sadeq H. Bakhy, and M.A. Tawfik, " Magnetic-type Climbing Wheeled Mobile Robot for Engineering Education " IOP Conference Series: Materials Science and Engineering, 2020. DOI: 10.1088/1757-899X/928/2/022145
[9] S. E. Sadiq, Sadeq H. Bakhy, and M. J. Jweeg, "Effects of spot welding parameters on the shear characteristics of aluminum honeycomb core sandwich panels in aircraft structure," Test Engineering and Management. Vol. 32, No. 7, pp. 7244 - 7255, 2020.
[10] S. E. Sadiq, Sadeq H. Bakhy, and M. J. Jweeg, "Crashworthiness behavior of aircraft sandwich structure with honeycomb core under bending load", IOP Conference Series: Materials Science and Engineering, 2020.
[11] S. K. Mahmood, Sadeq H. Bakhy, and M.A. Tawfik, "Novel wall-climbing robot capable of transitioning and perching " IOP Conference Series: Materials Science and Engineering, Vol. 881(1), 2020.
[12] R. A. Kadhim , E. M. Fayyadh and Sadeq H. Bakhy, " Stirrer speed control of a fluidized bed dryer for biomass particles using pwm technique," Plant Archives Vol. 20, Supplement 2, pp. 673-680, 2020.
[13] H. D. Salman, Sadeq H. Bakhy, and M. N. Hamzah 'Design and optimization of coupled and self-adaptive of an underactuated robotic hand using particle swarm optimization' 2nd International Scientific Conference of Al-Ayen University (ISCAU-2020), IOP Conference Series: Materials Science and Engineering, Vol. 928, 2020.
[14] Sadiq E. Sadiq, Muhsin J. Jweeg, and Sadeq H. Bakhy, 'The effects of honeycomb parameters on transient response of an aircraft sandwich panel structure' 2nd International Scientific Conference of Al-Ayen University (ISCAU-2020), IOP Conference Series: Materials Science and Engineering, Vol. 928, 2020.
[15] H. D. Salman, Sadeq H. Bakhy, and M.N. Hamzah, "Contact mechanics for soft hemi elliptical robotic fingertip" Journal of Mechanical Engineering Research and Developments Vol. 43No. 6, pp. 286-298, 2020.
[16] H. D. Salman, Sadeq H. Bakhy, and M.N. Hamzah, "Contact mechanics and nonlinear contacts stiffness for hemielliptical soft fingertip in grasping and manipulation" Journal of Mechanical Engineering Research and Developments, Vol. 44, No. 1, pp. 57-65, 2021.
[17] H. Kinoshita, L. Bäckström, J.R Flanagan, and R.S. Johansson, "Tangential torque effects on the control of grip forces when holding objects with a precision grip." Journal of Neurophysiology Vol. 78, No. 3, pp. 1619-1630, 1997.
[18] R. D. Howe, I. Kao, and M. R. Cutkosky, "The sliding of robot fingers under combined torsion and shear loading," Proceedings IEEE International Conference on Robotics and Automation, IEEE, 1988.
[19] Y. Li, and I. Kao, "A review of modeling of soft-contact fingers and stiffness control for dextrous manipulation in robotics," Proceedings ICRA. IEEE International Conference on Robotics and Automation (Cat. No. 01CH37164). Vol. 3. IEEE, 2001.
[20] M. Ciocarlie, A. Miller, and P. Allen, "Grasp analysis using deformable fingers." IEEE/RSJ International Conference on Intelligent Robots and Systems. IEEE, 2005.
[21] N. Elango, and R. Marappan, "Analysis on the fundamental deformation effect of a robot soft finger and its contact width during power grasping," The International Journal of Advanced Manufacturing Technology Vol.52, No. 5, pp. 797-804, 2011).
[22] B. Delhaye, Ph. Lefevre, and J. Thonnard, "Dynamics of fingertip contact during the onset of tangential slip," Journal of The Royal Society Interface Vol. 11, No.1, 2014.
[23] W. Miao, G. Li, G. Jiang, Y. Fang, Z. Ju, and H. Liu, "Optimal grasp planning of multi-fingered robotic hands: A review," Applied and Computational Mathematics, Vol. 14, No. 3. pp. 228–247, 2015.
[24] F. Yoshinori, K. Harada, T. Tsuji, and T. Watanabe, "Experimental investigation of effect of fingertip stiffness on resistible force in grasping," International Conference on Robotics and Automation (ICRA). IEEE, 2015.
[25] A. Fakhari, M. Keshmiri, and I. Kao, "Development of realistic pressure distribution and friction limit surface for soft-finger contact interface of robotic hands," Journal of Intelligent & Robotic Systems Vol. 82, No. 1,pp. 39-50, 2016.
[26] N. Xydas, and N. Kao, " Modeling of contact mechanics and friction limit surface for soft fingers in robotics, with experimental results," Int. J. Robot. Res. Vol.18, No.8, pp. 941–950, 1999.

[27] C. L. Mackenzie, and T. Iberall, "The grasping hand," Elsevier Science, Printed in The Netherlands, 1994
[28] A. Ikeda, Y. Kurita, J. Ueda, Y. Matsumoto, and T. Ogasawara, "Grip force control for an elastic finger using vision-based incipient slip feedback," Proceedings of IEEE/RSJ International Conference on Intelligent Robots and Systems, Vol. 1, pp. 810–815, 2004.
[29] J. Ueda, A. Ikeda, and T. Ogasawara, "Grip-force control of an elastic object by vision-based slip-margin feedback during the incipient slip," IEEE Trans. Robot. Vol. 21, No. 6, pp. 1139–1147, 2005.
[30] K.L. Johnson, "One hundred years of hertz contact," Proc. Institution Mech. Engineers Vol. 196, No. 1, pp.363–378, 1982.
[31] H. Hertz, "On the contact of rigid elastic solids and on hardness, Ch. 6" Assorted Papers (1882)
[32] Y. Tatara, "Large deformations of a rubber sphere under diametral compression: Part 1: Theoretical analysis of press approach, contact radius and lateral extension," JSME Int. J. 36(2), 190–196 (1993)
[33] S. P. Timoshenko and J. N. Goodier, "Theory of Elasticity", McGraw-Hill International Editions. 3rd edition, pp.414-420, 1970.
[34] S. H. Bakhy, S. S. Hassan, S. M. Nacy, K. Dermitzakis, and A. H. Arieta," Contact mechanics for soft robotic fingers: Modeling and experimentation", Robotica. Vol. 31, No. 04, pp. 599-609, 2013.
[35] I. Kao, and F. Yang, "Stiffness and contact mechanics for soft fingers in grasping and manipulation" IEEE Trans. Robot. Autom. Vol. 20, No. 1, pp.132–135, 2004. doi:10.1109/TRA.2003.820868
[36] S. Arimoto, P. Nguyen, H. Han, and Z. Doulgeri, "Dynamics and control of a set of dual fingers with soft tips. Robotica Vol.18, pp.71–80, 2000.
[37] B. H. Kim, "Motion analysis of soft-fingertip manipulation tasks" Int. J. Control. Autom. Syst. Vol. 2, No. 2, pp. 228–237. 2004.
[38] T. Inoue, S. Hirai,"Elastic model of deformable fingertip for soft-fingered manipulation", IEEE Trans. Robot. Vol. 22, pp.1273–1279, 2006.
[39] T. Inoue, S., Hirai, "Dynamic stable manipulation via softfingered hand", Proceedings of IEEE International Conference on Robotics and Automation, pp. 586–591, 2007.
[40] W. Flugge, "Viscoelasticity" Blaisdell Publishing Company, 1967.
[41] J. C. Maxwell, "On the dynamical theory of gases," Phil. Trans. R. Soc. London Vol. 157, pp. 49–88 1867.
[42] Y. C. Fung, "Biomechanics: mechanical properties of living tissues," Springer, 1993.
[43] P. Tiezzi and I. Kao, "Characteristics of contact and limit surface for viscoelastic fingers," Proceedings of IEEE International Conference on Robotics and Automation, pp. 1365–1370, 2006.
[44] P. Tiezzi and I. Kao, "Modeling of viscoelastic contacts and evolution of limit surface for robotic contact interface", IEEE Trans. Robot. Vol. 23, No. 2, pp. 206–217, 2007.
[45] S. H. Bakhy, " Modeling of contact pressure distribution and friction limit surfaces for soft fingers in robotic grasping", Robotica, Vol. 32. No. 7, pp. 1005 - 1015, 2014.
[46] M. Abramowitz, and I. Stegun, "Handbook of mathematical functions: with formulas, graphs, and mathematical tables," Applied Mathematics Series. Dover Publications, 1964.
[47] N. Xydas, and I. Kao, "Modeling of contact mechanics with experimental results for soft fingers," Proceedings of IEEE/RSJ International Conference on Intelligent Robots and Systems, Vol. 1, pp. 488-493, 1998.
[48] N. Xydas, and I. Kao, "Influence of material properties and fingertip size on the power-law equation for soft fingers," Proceedings of IEEE/RSJ International Conference on Intelligent Robots and Systems, Vol. 2, pp. 1285–1290, 2000.
[49] K. L. Johnson, " Contact Mechanics," Cambridge University Press, 1985.
[50] R. D. Mindlin, "Compliance of elastic bodies in contact," ASME J. Appl. Mechanics Vol.17, pp. 259–268, 1949.
[51] K. L. Johnson, " Surface interaction between elastically loaded bodies under tangential forces," Proc. R. Soc. Lond. A Math. Phys. Sci. Vol. 230, No. 1183, pp. 531–548, 1955.
[52] Y. Kurita, A. Ikeda, J. Ueda, Y. Matsumoto, and T. Ogasawara, " A novel pointing device utilizing the deformation of the fingertip," Proceedings of IEEE/RSJ International Conference on Intelligent Robots and Systems, Vol. 1, pp. 13–18, 2003.
[53] Y. Kurita, A. Ikeda, J. Ueda, and T. Ogasawara, "A fingerprint pointing device utilizing the deformation of the fingertip during the incipient slip," IEEE Trans. Robot. Vol. 21, No. 5, pp. 801–811, 2005.
[54] S. Goyal, A. Ruina, and J. Papadopoulos, "Planar sliding with dry friction: Part 1. limit surface and moment function," Wear, Vol. 143, pp. 307–330, 1991.
[55] R. Howe and M. Cutkosky, "Practical force-motion models for sliding manipulation," Int. J. Robot. Res. Vol. 15, No.6, pp. 555–572, 1996.
[56] Saif M. Abbas, Ayad M. Takhakh, Mohsin Abdullah Al-Shammari, and Muhannad Al-Waily 'Manufacturing and Analysis of Ankle Disarticulation Prosthetic Socket (SYMES)' International Journal of Mechanical Engineering and Technology (IJMET), Vol. 09, No. 07, pp. 560-569, 2018.
[57] Saif M. Abbas, Kadhim K. Resan, Ahmed K. Muhammad, and Muhannad Al-Waily 'Mechanical and fatigue behaviors of prosthetic for partial foot amputation with various composite materials types effect' International Journal of Mechanical Engineering and Technology (IJMET), Vol. 09, No. 09, pp. 383–394, 2018.
[58] Muhsin J. Jweeg, Muhannad Al-Waily, Ahmed K. Muhammad, and Kadhim K. Resan 'Effects of temperature

on the characterisation of a new design for a non-articulated prosthetic foot' IOP Conference Series: Materials Science and Engineering, Vol. 433, 2nd International Conference on Engineering Sciences, Kerbala, Iraq, 26–27 March, 2018.

[59] Ehab N. Abbas, Muhsin J. Jweeg, and Muhannad Al-Waily 'Fatigue characterization of laminated composites used in prosthetic sockets manufacturing' Journal of Mechanical Engineering Research and Developments, Vol. 43, No. 5, pp. 384-399, 2020.

[60] Ehab N. Abbas, Muhannad Al-Waily, Tariq M. Hammza, and Muhsin J. Jweeg 'An investigation to the effects of impact strength on laminated notched composites used in prosthetic sockets manufacturing' IOP Conference Series: Materials Science and Engineering, 2nd International Scientific Conference of Al-Ayen University, Vol. 928, 2020.

[61] Muhannad Al-Waily, Moneer H. Tolephih, and Muhsin J. Jweeg 'Fatigue characterization for composite materials used in artificial socket prostheses with the adding of nanoparticles, IOP Conference Series: Materials Science and Engineering, 2nd International Scientific Conference of Al-Ayen University, Vol. 928, 2020.

[62] Muhsin J. Jweeg, Zaid S. Hammoudi, and Bassam A. Alwan 'Optimised analysis, design, and fabrication of trans-tibial prosthetic sockets' IOP Conference Series: Materials Science and Engineering, 2nd International Conference on Engineering Sciences, Vol. 433, 2018.

[63] Muhsin J. Jweeg, Abdulkareem Abdulrazzaq Ahumdany, and Ali Faik Mohammed Jawad 'Dynamic stresses and deformations investigation of the below knee prosthesis using ct-scan modeling' International Journal of Mechanical & Mechatronics Engineering IJMME-IJENS, Vol. 19, No. 01, 2019.

[64] Ayad M. Takhakh, Saif M.Abbas, and Aseel.K. Ahmed 'A Study of the mechanical properties and gait cycle parameter for a below-knee prosthetic socket' IOP Conference Series: Materials Science and Engineering, 2nd International Conference on Engineering Sciences, Vol. 433, 2018.

[65] Fahad M. Kadhim, Ayad M. Takhakh, and Asmaa M. Abdullah 'Mechanical properties of polymer with different reinforcement material composite that used for fabricates prosthetic socket' Journal of Mechanical Engineering Research and Developments, Vol. 42, No. 4, pp. 118-123, 2019.

[66] Lara E. Yousif, Kadhim K. Resan, and Raad M. Fenjan 'Temperature effect on mechanical characteristics of a new design prosthetic foot' International Journal of Mechanical Engineering and Technology (IJMET), Vol. 09, No. 13, pp. 1431-1447, 2018.

[67] Fahad M. Kadhim, Jumaa S. Chiad, and Maryam Abdul Salam Enad 'Evaluation and analysis of different types of prosthetic knee joint used by above knee amputee' Defect and Diffusion Forum Journal, Vol. 398 , pp. 34–40, 2020.

[68] Fahad M. Kadhim, Ayad M. Takhakh, and Jumaa S. Chiad 'Modeling and evaluation of smart economic transfemral prosthetic' Defect and Diffusion Forum Journal, Vol. 398, pp. 48–53, 2020.

[69] Fahad M Kadhim, Jumaa S Chiad, and Ayad M Takhakh 'Design and manufacturing knee joint for smart transfemoral prosthetic' IOP Conference Series: Materials Science and Engineering, International Conference on Materials Engineering and Science, Vol. 454, 2018.

[70] Bashar A. Bedaiwi, and Jumaa S. Chiad 'Vibration analysis and measurement in the below knee prosthetic limb part I: Experimental work' ASME 2012 International Mechanical Engineering Congress and Exposition, Proceedings (IMECE), 2012.

[71] Jumaa S. Chiad 'Study the impact behavior of the prosthetic lower limb lamination materials due to low velocity impactor' ASME 2014 12th Biennial Conference on Engineering Systems Design and Analysis, ESDA, 2014, July 25–27, 2014.

[72] J. K. Oleiwi, and A. N. Hadi 'Experimental and numerical investigation of lower limb prosthetic foot made from composite polymer blends' International Journal of Mechanical and Production Engineering Research and Development, Vol. 08, No. 02, pp. 1319-1330, 2018.

[73] A. Z. Mahdi, S. A. Amin, and Sadeq H. Bakhy, "Influence of Refill Friction Stir Spot Welding Technique on the Mechanical Properties and Microstructure of Aluminum AA5052 and AA6061-T3," IOP Conference Series: Materials Science and Engineering 671, 2020.

[74] S. I. Salih, J. K. Oleiwi, and H. M. Ali 'Study the mechanical properties of polymeric blends (SR/PMMA) using for maxillofacial prosthesis application' International Conference on Materials Engineering and Science, IOP Conference Series: Materials Science and Engineering, Vol. 454, 2018.